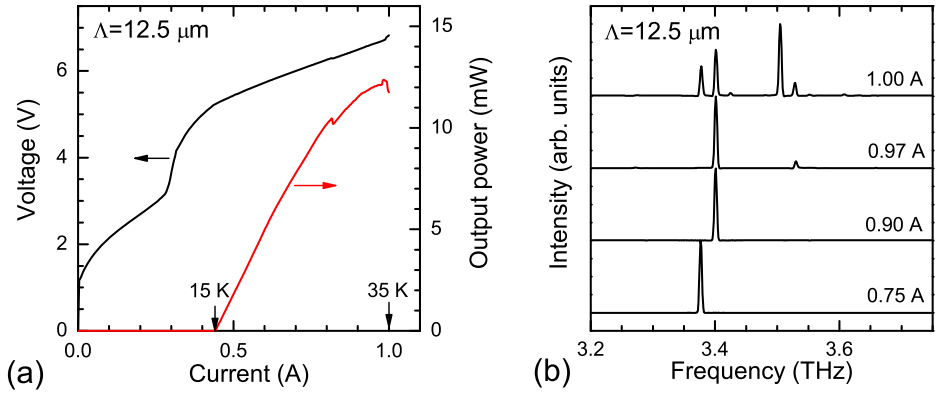

Fig. 4. (a) Continuous-wave *L-I-V* characteristics for the lDFB QCL with $\Lambda = 12.5\ \mu$m including the multi-mode emission regime (disabled temperature control loop). (b) Corresponding emission spectra at four different driving currents.

small as a few kHz for THz QCLs [26], cannot be determined from the spectra due to the limited resolution of the used spectrometer (Bruker, IFS66v). The instrumental resolution allows for a clear identification of modes, which are separated by more than 3.5 GHz. The question may arise, if these spectra consist of different transverse modes which are not resolved. However, we disregard this possibility for a simple reason. According to the simulation results discussed above, the effective index for the TM_{00} and TM_{01} mode differ by 1.2%, which causes a shift of the Bragg frequency from 3.33 to 3.37 THz. Hence, the longitudinal mode with the lowest threshold gain is expected to differ by more than 40 GHz for TM_{00} and TM_{01} symmetry, which is well beyond the resolution limit. In contrast, higher-order transverse modes are likely to explain the complicated multi-mode emission spectra observed at elevated driving currents.

From beam-profile measurements for one of the lDFB lasers operated in a Stirling cooler, we found that the far field is very similar to single-plasmon lasers without a grating (cf. Ref. [6]). For a driving current of 600 mA and operating temperature of 50 K, the beam profile of the $\Lambda = 12.4\ \mu$m laser consists mainly of a single lobe, covering approximately 80% of the power, for which we estimate a full width at half maximum divergence of about 24° in both, the lateral and the vertical, directions. The beam divergence appears to be comparable to the one of third-order DFB QCLs, for which values of 15 to 30° have been reported [16].

In Fig. 4(a), the *L-I-V* characteristics are shown for the laser with $\Lambda = 12.5\ \mu$m including the multi-mode emission regime. Due to the large dissipated electrical power at elevated current levels, the temperature control loop was disabled for this measurement resulting in a linear temperature increase of 20 K between the threshold and the maximum applied current of 1.0 A. At its maximum, the cw output power exceeds 12 mW for this laser. In Fig. 4(b), the emission spectra for different operating currents are shown. Between 0.75 and 0.9 A, the laser emission switches from 3.38 to 3.40 THz. This new regime is related to a discontinuity at 0.82 A in the light-current characteristics, which is also observed in the *I-V* characteristics. When the driving current is increased to 0.97 A, another mode at 3.53 THz starts to appear, and, at a driving current of 1.0 A, the laser emission exhibits a complex multi-mode pattern with strong modes at 3.38/3.40 THz and 3.50/3.53 THz.

The emission spectra can be interpreted within the framework of the coupled-mode equations for a DFB cavity (see Appendix) with the boundary condition of two reflective end facets, for which the facet phases as defined in Fig. 1(a) enter the eigenvalue problem. The coupled-mode

#159974 - $15.00 USD Received 15 Dec 2011; revised 4 Mar 2012; accepted 10 Apr 2012; published 1 May 2012

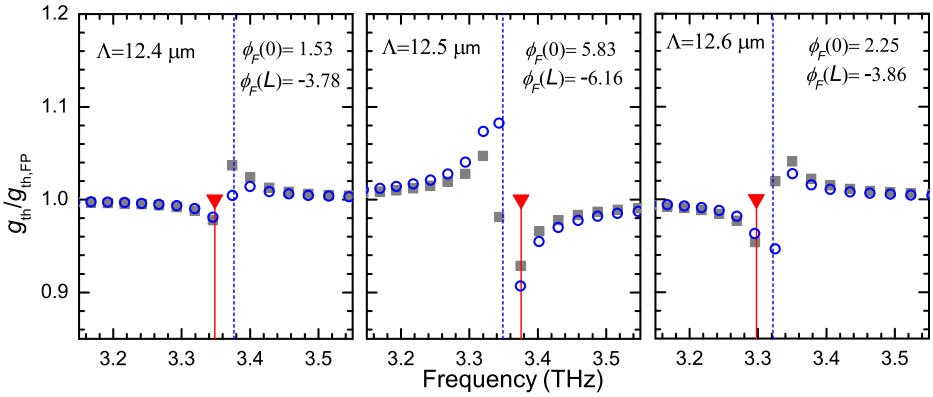

Fig. 5. Calculated threshold gain g_{th} vs. frequency of the eigenmodes of the lDFB lasers ($\Lambda = 12.4$, 12.5, and 12.6 μm) in units of g_{th} of the reference Fabry-Pérot cavity. The vertical dashed lines indicate the Bragg frequency using $n = 3.58$. The facet phases ϕ_F as defined in Fig. 1(a) have been determined by SEM imaging and are given in radians. Circles refer to a complex coupling coefficient [$K + iK_g = (3.0 + 0.8i)$ cm^{-1}] and squares to a real coupling coefficient ($K = 3.0$ cm^{-1}). Triangles indicate the experimentally observed frequencies.

equations have been solved numerically for this case. In Fig. 5, the calculated threshold gain for the TM_{00} mode is plotted versus the frequency eigenvalues for the three lDFB QCLs with $\Lambda = 12.4$, 12.5, and 12.6 μm. We have performed simulations either for a complex coupling coefficient or for a real coupling coefficient ($K_g = 0$). The experimentally observed single-mode emission and the calculated longitudinal modes with the lowest threshold gain occur at almost the same frequencies, where the quantitative agreement appears to be better for the simulations with a real coupling coefficient. In this case, an agreement better than 9 GHz is found for all three lasers, while in the case of a complex coupling coefficient the calculated mode with the second lowest threshold gain coincides with the lasing frequency for $\Lambda = 12.6$ μm. While the Bragg frequency (depicted as dashed lines in Fig. 5) decreases with increasing grating period, the finite facet reflectance and the different facet phases cause lasing in the longitudinal mode below the Bragg frequency for $\Lambda = 12.4$ and 12.6 μm and above the Bragg frequency for $\Lambda = 12.5$ μm. The differences in the calculated threshold gain explain the different experimentally observed threshold current densities. However, the calculation predicts the lowest threshold gain for $\Lambda = 12.5$ μm, while experimentally the lowest value of J_{th} is found for $\Lambda = 12.6$ μm [cf. Fig. 3(a)]. Differences between the experimental and simulated results are likely due to the uncertainty of the involved parameters such as the coupling coefficients. For instance, the occurrence of a small displacement between the etch mask and the metallization mask might result in a phase difference between the index and gain coupling, which has been neglected in the simulations.

While the single-mode operation regime is quite well explained by the coupled-mode equations for the fundamental lateral TM_{00} mode, the situation becomes more complex for the multi-mode emission regime. In Fig. 4(b), the emission of a second mode at 3.40 THz for the laser with $\Lambda = 12.5$ μm can be understood by the Stark shift of the gain with increasing bias, since the emission frequency agrees with the calculated frequency of the mode with the second lowest threshold gain. However, the multi-mode emission pattern for the highest driving current seems to exhibit a stop band between 3.40 and 3.50 THz. This cannot be explained by the

#159974 - $15.00 USD Received 15 Dec 2011; revised 4 Mar 2012; accepted 10 Apr 2012; published 1 May 2012

spectral position and threshold gain of the longitudinal modes with TM_{00} symmetry. A likely explanation is the presence of higher-order lateral modes such as TM_{01} and TM_{02}, for which the coupling coefficient is much larger and the Bragg frequency is increased due to the smaller effective index of these modes. For lasing of higher-order lateral modes in favor of the fundamental TM_{00} mode, the threshold gain has to be smaller as compared to the TM_{00} mode, i.e. the larger coupling coefficient has to compensate the higher waveguide losses.

4. Summary and conclusions

We have demonstrated THz QCLs based on first-order lateral DFB gratings and single-plasmon waveguides, which operate in continuous-wave mode with high output powers and single-mode emission around 3.3 THz. For the single-mode regime, cw output powers exceeding 8 mW have been obtained, while the maximum output power including the multi-mode regime can exceed even 12 mW. A method has been developed to calculate the coupling strength of DFB gratings in the presence of corrugated metal layers, which demonstrates that the origin of the large coupling strength in the investigated lasers is the strong plasmonic metal-light interaction at the lateral grating edges. The emission frequency of the lasers is determined by the Bragg frequency of the grating and the positions of the cleaved facets with respect to the grating comb. By taking into account the reflective end facets, a quantitative agreement between the experimental spectra and simulations based on the coupled-mode equations of DFB lasers is obtained. The present approach is limited by the accuracy of the cleaving process, which causes an uncertainty of the emission frequency approximately equal to the mode spacing of the corresponding Fabry-Pérot cavity. However, the number of mounted laser dies, which have to be tested to obtain a particular target frequency, can be kept small if laser ridges with different grating periods are located on the same die.

5. Appendix

In order to derive Eq. (1), we start with the coupled-mode equations following the notation of Ref. [21]:

$$\frac{d}{dz}\begin{pmatrix}A(z)\\B(z)\end{pmatrix} = i\begin{pmatrix}\Delta\beta & K_{ab}\\ -K_{ba} & -\Delta\beta\end{pmatrix}\begin{pmatrix}A(z)\\B(z)\end{pmatrix}. \tag{4}$$

$A(z)$ and $B(z)$ denote the amplitudes of the forward and backward propagating wave, respectively. K_{ab} and K_{ba} refer to the coupling coefficients of the forward and backward propagating mode, respectively, and $\Delta\beta = \beta_0 - \beta_B$ corresponds to the difference of the propagation constant $\beta_0 = \omega n_{\text{eff}}/c$ and the Bragg wavevector $\beta_B = \pi/\Lambda$. The coupled-mode equations in Eq. (4) are formally solved by

$$\begin{pmatrix}A(z)\\B(z)\end{pmatrix} = \begin{pmatrix}A_\pm\\B_\pm\end{pmatrix} e^{\pm iqz} \tag{5}$$

with

$$q = \sqrt{\Delta\beta^2 - K_{ab}K_{ba}}\,. \tag{6}$$

The latter equation is the dispersion relation for the coupled system of forward and backward propagating waves of a uniform grating of infinite length. The propagation constant of the coupled system are given by $\beta_\pm = \pi/\Lambda \pm q$, while β_0 and $\Delta\beta$ refer to the reference waveguide. Note that q, β_0, and $\Delta\beta$ are complex quantities in the current notation due to the presence of gain and losses, while the frequency ω is a real quantity.

In the case of index and gain coupling, the coupling coefficients can be written as $K_{ab} = K + iK_g\exp(i\phi_g)$ and $K_{ba} = K + iK_g\exp(-i\phi_g)$ with K denoting the index coupling coefficient,

#159974 - $15.00 USD Received 15 Dec 2011; revised 4 Mar 2012; accepted 10 Apr 2012; published 1 May 2012

K_g the gain coupling coefficient, and ϕ_g the phase difference between index and gain coupling. We obtain the relation

$$K_{ab}K_{ba} = K^2 - K_g^2 + 2iKK_g\cos(\phi_g)\ . \tag{7}$$

Here, only symmetric gratings are considered, for which the origin in the ridge direction z can be chosen such that $\Delta\varepsilon(z) = \Delta\varepsilon(-z)$. The only possible values for ϕ_g are 0 and π, $K_{ab}K_{ba} = (K \pm iK_g)^2$, where we chose the plus sign in the following by allowing for negative amplitudes K_g. We rewrite Eq. (6) using $\omega = \beta_0 c/n_{\text{eff}} = \beta_0 c/(n+ik)$:

$$\omega_{\pm}(q) = \frac{c}{n+ik}\left(\frac{\pi}{\Lambda} \pm \sqrt{q^2 + K_{ab}K_{ba}}\right)\ . \tag{8}$$

In the following, the wavevector $\pi/\Lambda \pm q$ is treated as a real quantity, which causes β_0 and $\Delta\beta$ to be real, while the frequency ω becomes complex. The case $q = 0$ correspond to the eigenfrequencies of a one-dimensional photonic crystal at the edge of the Brillouin zone. Assuming a symmetric grating with $K_{ab}K_{ba} = (K + iK_g)^2$, the complex frequencies of the two eigenmodes at $q = 0$ are given by Eq. (1).

Acknowledgment

The authors would like to thank M. Höricke for sample growth, W. Anders for sample processing, H. Ogiya (SAMCO Inc.) for dry etching, H. Wenzel (FBH Berlin) for the numerical tool to solve the coupled-mode equations, and H. Richter (DLR Berlin) for providing the beam profile measurements. We also acknowledge partial financial support by the European Commission through the ProFIT program of the Investitionsbank Berlin.

#159974 - $15.00 USD Received 15 Dec 2011; revised 4 Mar 2012; accepted 10 Apr 2012; published 1 May 2012